Special Issue on "Theoretical and Computational Chemistry"

J. Indian Chem. Soc.,
Vol. 96, July 2019, pp. 909-919

Density Functional Theory study on the formation of the active catalysts in palladium catalysed reaction

Davuluri Yogeswara Rao and Anakuthil Anoop*

Department of Chemistry, Indian Institute of Technology Kharagpur, Kharagpur-721 302, West Bengal, India

E-mail: anoop@chem.iitkgp.ac.in

Manuscript received online 03 May 2019, revised and accepted 22 May 2019

The formation of active catalyst species in the Pd-catalyzed reactions is studied using Density Functional Theory calculations. Taking palladium acetate and simple phosphine as the models, we estimated the energetics for the addition of phosphines, release of acetates, and associative exchange or ligands which convert the unreactive $PdOAc_2$ to reactive species that takes part in the catalysis. Two consecutive addition of two phosphines, $PdOAc_2 + 2PH_3 \rightarrow Pd(OAc)_2(PH_3)_2$ are exergonic steps with the free energies of activation 8.16 kcal mol^{-1} and 5.33 kcal mol^{-1}. The associative exchange of acetate by PH_3 in $Pd(OAc)_2(PH_3)_2$ has 14.56 kcal mol^{-1} of activation barrier, while the exchange in $[Pd(OAc)(PH_3)_3]^-$ has the barrier of 5.22 kcal mol^{-1}. Exchange reactions on neutral species that yields ionic species are endothermic in gas phase which is drastically reduced by solvation model. The addition of phosphines are exothermic. The dissociative steps are the removal of acetate anion, AcO^-, or intramolecular dissociation of $[AcO\text{-}PH_3]^+$. This study is a basis for future studies of the active catalyst formation of various such catalysts involving different ligands.

Keywords: DFT, active catalyst formation, Pd-catalysed reaction, ligand exchange reactions, computational study.

Introduction

Palladium catalyzed coupling reactions – Heck[1,2], Negshi[3,4], Suzuki[5–7], Stille[8], and so on – are widely used for making carbon-carbon and carbon-heteroatom bonds. The common catalysts used in these coupling reactions are, $Pd(OAc)_2$, $Pd(PR_3)_4$, $PdCl_2(PR_3)_2$, etc. These materials act as pro-catalysts or pre-catalysts, which *in situ* gets converted to the active catalyst species in the catalytic cycle. The active-catalysts are coordinatively unsaturated Pd complexes with one, two, or three ligands. The activity of each of these species may be different, and can have significant impact on the overall catalytic efficiency. In some cases, as shown by computational studies, each species may follow separate pathways in the catalytic cycle[9]. The steps involved in the formation of active catalyst is much less explored compared to the studies on the catalytic cycle, although the identity of active catalyst is crucial in understanding the mechanism.

The attempts to experimentally detect the species in the Pd catalysis were pioneered by the seminal works by Christian Amatore *et al.*[10–14] on neutral catalysts and by John D. Protasiewicz and co-workers on ionic catalysts[15,16]. Amatore *et al.* have explained how zero-valent palladium is formed from divalent palladium triphenylphosphine complexes with the help of $^{\{31\}}P$ NMR and cyclic voltammetry to detect and characterize. Later, they traced the reactive mono-phosphine-ligated palladium intermediates by mass spectrometry in the Pd-catalyzed coupling reaction[17]. These works provide some valuable insight for the proposed steps towards the catalyst formation which is shown in Fig. 1. Amatore and Jutand reported the finding of the intermediate species by electrochemical techniques where reduction and oxidation process occur.

The importance of ligation states are established by numerous computational studies on Pd-catalyzed reactions. The steric and electronic properties of the ligands decide which ligation states are favourable for each reaction. The commonly studied Pd-catalyst is PdL[18–26], or Pd-L_2[27,28]. In some studies, the mechanism starts with PdL_2 and becomes PdL along the pathway[29–33]. A tetrahedral Pd(0)-catalyst is formed before the formation of activated Pd(0) pre-catalysts. Tamas Kegl *et al.* studied the formation of PdL by step-by-step dissociation of L_4Pd[28] using Density Functional Theory (DFT)

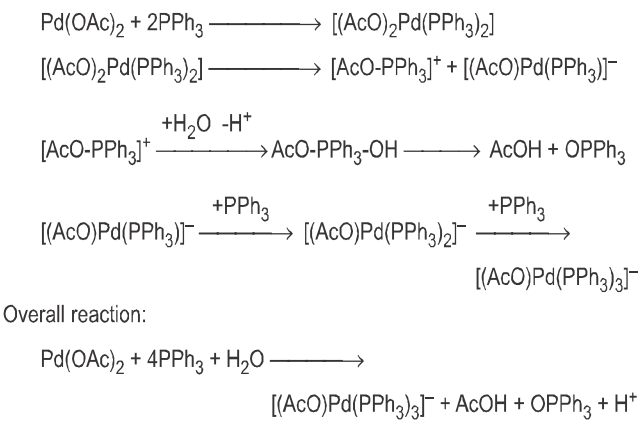

Fig. 1. Steps in the formation of active catalyst species based on the experiments.

calculations. Two distinct mechanistic pathways of the Pd-catalysed reactions, ionic, and neutral, are established by DFT methods[34]. Norrby and co-workers concluded that, the ionic path is expected to be competitive with the neutral path even in the presence of small amounts of ionic ligands. Bottoni *et al.*[35] studied the reduction of palladium(II) in $Pd(OAc)_2$ complexes reacting with triphenylphosphines and leading to $Pd(0)(PPh_3)_4$ complexes mainly focusing on the neutral pathways.

Despite their enormous synthetic and theoretical importance, the mechanism of the early events in the catalysis is still not fully understood. In this work, we are exploring the possible steps in the formation of active catalyst species using Density Functional Theory calculations. These elementary steps convert the palladium acetate, $Pd(AcO)_2$, to the pre-catalyst species, L_xPd, $L_xPd(AcO)_y$; x = 1–4, y = 1–2, and L = PH_3. We employed gas-phase models and implicit solvation models for anionic and neutral catalysts that are shown to be present during the experiments. This work is expected to be a basis for more detailed studied on the effects of various ligands on these steps.

Computational methods

The general procedure followed for finding the reaction profile and the transition state is described below. We have carried out a relaxed surface scan with Pd-P distance as the reaction coordinate. In each step of the scan, the Pd-P distance was kept constant and all other coordinates were fully optimized. The step size was 0.5 Å, i.e. the Pd-P distance was decreased by 0.5 Å after each step. The last point in the scan was fully optimized without any constraints to find the geometry of the product of each step-wise reaction which are intermediates in the catalytic cycle. After we got the optimized geometries of both ends – reactant and product of each step – we have optimized a minimum energy path between these two points using NEB method[36] and the highest energy point was further optimized for a transition state using Climbing Image algorithm. In cases where NEB failed to converge, we have used dimer method[37] to locate the TS. All the above steps were carried out using DL-Find module[38] implemented in ChemShell[39].

The transition state geometry obtained by the above procedure was further optimized by the transition state searching methods in the statpt module of Turbomole[40]. A vibrational frequency analysis was done on optimized geometries using AOFORCE module[41,42] from Turbomole. We characterized all the geometries with vibrational frequency calculations; the reactants and intermediates were distinguished as minima with no negative imaginary frequency and the transition states contained one negative imaginary frequency corresponding to the reaction mode. The nature of transition states were confirmed by additional intrinsic reaction coordinate (IRC)[43] calculations using DRC module implemented in Turbomole. The free energy corrections calculated through the vibrational analysis is used for calculating the free energy changes in the reaction.

We performed all DFT calculations with Turbomole[40] program package. The geometries were optimized with BP86[44,45] functional and def2-SVP[46] basis sets along with resolution of identity (RI) approximation[47] for speed up and to account for dispersive interactions. The default effective core potentials (def2-ecp) implemented in Turbomole was used for P and Pd which also accounts for the relativistic effects[48,49]. To compare the results with functionals other than BP86, single point calculations were carried out using hybrid B3LYP functional[50] and meta-hybrid M06[51] functional with the same basis set. For the solvent effect, the single-point calculations on the optimized gas-phase geometries with COSMO solvation model was done (solvent = dimethylformamide (DMF, dielectric constant ($\in$) = 36.7).

Results and discussions

The materials modeled in this study are palladium acetate ($PdOAC_2$) and simple phosphine (PH_3). We studied

the possible steps leading to the active catalyst species. The first two steps are the consecutive addition of two phosphine ligands to palladium acetate. The $Pd(OAc)_2(PH_3)_2$ undergoes dissociation or exchange of acetate ligands to form various active catalyst species.

Consecutive addition of two phosphines to Pd(OAc) $_2$

The first two steps (eq. (1)), the consecutive addition of two phosphines, are relatively straightforward steps where the η^2 coordination of acetate is converted to η^1 and the vacancy in the coordinate is filled by the incoming phosphine ligands. There is no change in the oxidation state of Pd(II) in these steps. We describe these steps in this section.

$$PdOAc_2 + 2PH_3 \rightarrow Pd(OAc)_2(PH_3)_2 \quad (1)$$

When we carried out a relaxed surface scan along the Pd-P bond distance as the reaction coordinate, we have located a stable minimum ([**00_INT**]) in which the phosphine is weakly bound to Pd. Phosphine occupy the axial position of the square-planar $Pd(OAc)_2$. The stabilization achieved in the case of most addition reactions, a weakly bound complex of two reactants is expected. By this interaction of phosphine with $Pd(OAc)_2$ is –5.79 kcal mol^{-1}. The Gibbs free energy, however, is increased by 3.61 kcal mol^{-1} due to the decrease in entropy.

The optimized geometry of [**00_INT**] indicate non-covalent interaction between PH_3 and Pd (Fig. 2). The Pd-P bond distance is 3.11 Å, much longer than the Pd-P bond length of 2.24 Å (in [**02_INT**]). The interaction does not affect the Pd-O bond distances, 2.07 Å in [**00_INT**] and in free palladium acetate. There is no deviation from the square-planar geometry after the coordination of phosphine. All the angles, ∠P-Pd-P, are close to 90°. Thus, phosphine is only weakly bound to the palladium acetate complex in [**00_INT**].

We continued the relaxed surface scan from [**00_INT**] with Pd-P distance as the reaction coordinate (see Computational methods section for details). As the P atom approach Pd, one of the Pd-O bond got elongated. The last point in the scan was fully optimized without any constraints to find the optimized geometry of the intermediate $Pd(\eta^2\text{-}OAc)(\eta^1\text{-}OAc)(PH_3)$ ([**02_INT**]). The geometries of intermediates and transition state ([**01_TS**]) in this step are shown in Fig. 3. The other geometric changes associated with this step are the detailed in the Supporting Information. During this step, phosphine moves from the axial position to one of the square-planar position that was previously occupied by an oxygen of the acetate ligand, and the Pd-O bond has broken.

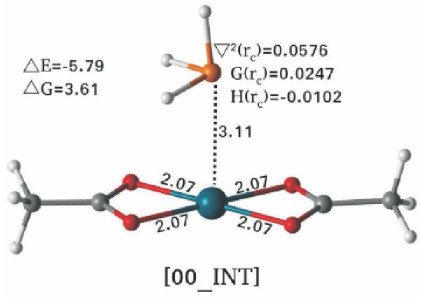

Fig. 2. The optimized geometry of [**00_INT**]. The relevant bond distances (in Å) and topological parameters from QTAIM analysis are shown.

The Gibbs free energy or reaction $\Delta_r G$ can be calculated either from the free separate reactants, i.e. $Pd(OAc)_2 + PH_3 \rightarrow$ [**02_INT**], or from the bound complex, i.e. [**00_INT**] $\rightarrow$ [**02_INT**]. These two $\Delta_r G$'s are distinguished in this report as $\Delta_r G^{Free}$ and $\Delta_r G^{Bound}$. This step is exergonic, $\Delta_r G^{Bound}$ = –15.12 kcal mol^{-1}, and exothermic, $\Delta_r E^{Bound}$ = –28.66 kcal mol^{-1} from [**00_INT**]. The corresponding values for $\Delta_r G^{Free}$ is –18.73 and $\Delta_r E^{Free}$ is 22.88 kcal mol^{-1}. The free energy of activation ($\Delta^{\ddagger} G^{Free}$) is 8.16 kcal mol^{-1} from the free reactants and 3.62 kcal mol^{-1} from [**00_INT**] ($\Delta^{\ddagger} G^{Bound}$). Hence, the addition of the first phosphine to palladium acetate is exothermic and has a relatively low barrier at BP86-D3/def2-

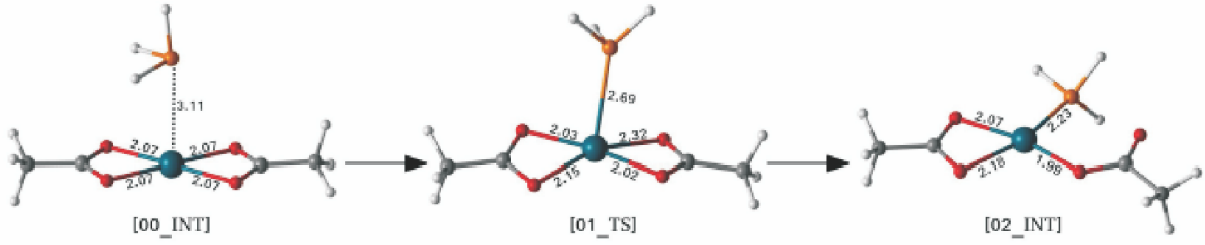

Fig. 3. Optimized geometry of [**01_TS**] and [**02_INT**], the transition and the product of the addition of PH_3 to $Pd(OAc)_2$.

SVP level in gas phase. We have examined the variations of these energies with other density functionals, and with the inclusion of implicit solvation models. The free energy of activation, $\Delta^{\ddagger}G^{Free}$, is higher, 11.6 kcal mol^{-1} in B3LYP, and 9.3 kcal mol^{-1} in M06 single point calculations. These variations are in line with and in the range of the expected variations among the DFT functionals. The effect of solvation is marginal. The full data is provided in Supporting Information.

Similar to the first addition discussed above, the insertion of the second phosphine goes through a weakly bound complex between [**02_INT**] and PH_3. This binding of PH_3 provides a stabilization of 6.69 kcal mol^{-1} to [**03_INT**]. The free energy, however, is increased by 3.73 kcal mol^{-1}. The Pd-P distance with the new phosphine is slightly shorter (3.07 Å) compared to that in [**00_INT**], in accordance with approximately 1 kcal mol^{-1} increase in the stabilization energy. The details of geometric and topological parameters are given in Supporting Information.

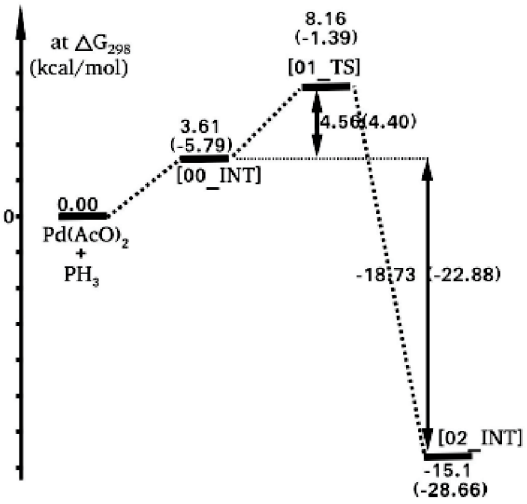

Fig. 4. Reaction profile for addition of PH_3 to $Pd(OAc)_2$. Relative free energies are given for each states in the reaction. The numbers in parentheses are relative total energies. Energies are in kcal mol^{-1}.

We studied the addition of the second phosphine following the same procedure used for the first step. During the relaxed surface scan, along with the shortening of Pd-P bond, one of the Pd-O bonds corresponding to the oxygen in the *trans* position to the first coordinated phosphine was elongated. Thus, the second η^2 acetate also became monodentate. The end point of this scan after free-optimization is $Pd(OAc)_2(PH_3)_2$ ([**05_INT**]). The [**05_INT**] has two phosphines *trans* to each other, and two monodentate acetates occupy the other *trans* positions. The uncoordinated oxygens of acetate ligands are also in the plane of the complex.

The optimized geometries of [**04_TS**] and [**05_INT**] are shown in Fig. 6. The activation free energy ($\Delta^{\ddagger}G^{Free}$) is 5.33 kcal mol^{-1}. The transition state ([**04_TS**]) is only 1.8 kcal mol^{-1} higher in free energy compared to [**03_INT**], indicating an almost spontaneous reaction. The reaction energy for this step ($\Delta_r G^{Free}$), is –10.16 kcal mol^{-1}. Thus, this step is exergonic with a small activation energy. The solvent effect, from the calculation with COSMO solvation model with DMF as solvent, is marginal for the first and second additions of phosphines (see Supporting Information), apparently as the molecules are neutral.

The additions of two phosphine molecules are exothermic and involves relatively low barriers. The bidentate coordination of both acetates is changed to monodentate coordination that create coordination space for the incoming phos-

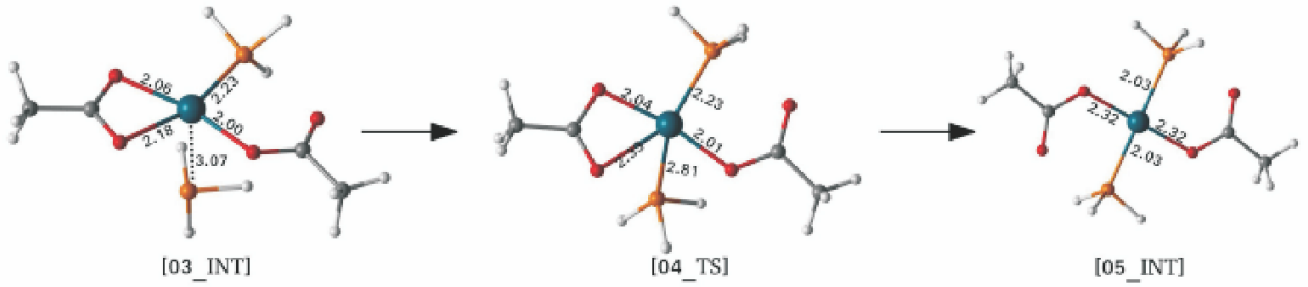

Fig. 5. Optimized geometry of weakly bound complex [**03_INT**], transition state [**04_TS**], and the product [**05_INT**] of the addition of PH_3 to $Pd(OAc)_2(PH_3)$.

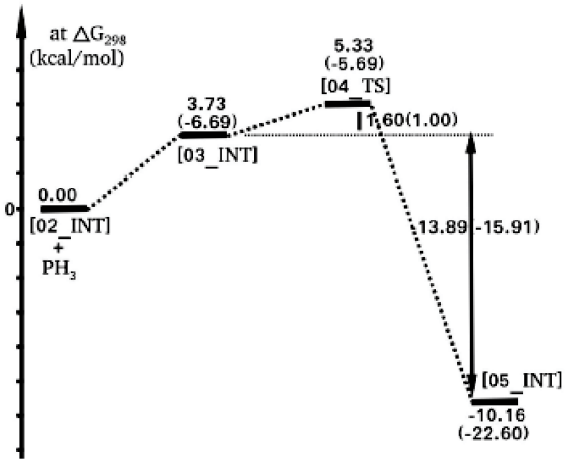

Fig. 6. Reaction profile for addition of PH_3 to Pd(η^2-OAc)(η^1-OAc)PH_3. Relative free energies are given for each states in the reaction. The numbers in parentheses are relative total energies. Energies are in kcal mol^{-1}.

phines. The overall free energy of reaction (eq. (1)) is –25.29 kcal mol^{-1}. The second addition is easier than the first one as per the barriers. The Pd(II)$(OAc)_2(PH_3)_2$ ([**03_INT**]) is a tetra-coordinate species and is not an active catalyst. The steps leading to the generation of active catalyst species is discussed in the following sections.

Formation of active catalysts

We can envisage many pathways from $Pd(OAc)_2(PH_3)_2$ ([**05_INT**]) that can lead to the formation of the following potential active catalysts. The species that contain only phosphines are $Pd(PH_3)_n$; n = 1–3. The anionic pathways involve anionic $Pd(OAc)(PH_3)_n^-$; n = 0–2. Substitution of both acetates will generate the inactive $Pd(PH_3)_4$. Any further addition of phosphine to [**05_INT**] is expected to replace the existing ligands as the stable coordination number of Pd is four. The ligand-exchange of AcO^- with PH_3, or dissociation of AcO^- will cause a change in oxidation states of Pd. The addition or dissociation of PH_3 maintain the oxidation state. We analyzed the pathways for the associative ligand exchange reactions and calculated the free energies of activation, while only the free energies of reactions are calculated for dissociation reactions.

We analyzed the first ligand exchange of acetate by phosphine (eq. (2)) by the same procedure we followed for the first two steps, i.e. insertion of PH_3 to [**05_INT**]. The weakly bound complex of [**06a_INT**] is stabilized by –8.33 kcal mol^{-1} (–7.69 in DMF). As in the previous cases, the free energy of the system has increased by 3 kcal mol^{-1}. The bond distance of the Pd to the incoming phosphine is 3.11 Å. While the Pd-P bond distances are similar to the first two phosphine bound complexes, the stabilization is higher.

$$PdOAc_2(PH_3)_2 \xrightarrow[-OAc^-]{+PH_3} [Pd(OAc)(PH_3)_3]^+ \qquad (2)$$

On carrying out the relaxed surface scan of reducing the Pd-P distance in [**06a_INT**], one of the acetates gets dissociated from the complex. The activation free energy for this ligand exchange of acetate by phosphine is 14.56 kcal mol^{-1} (13.24 in DMF). This barrier is higher compared to the first two additions (8.2 and 5.3 kcal mol^{-1}). The solvation is starting to show some effect, the barrier is lower by 1.5 kcal mol^{-1} with COSMO. In the transition state [**07a_TS**], the Pd-P distance of the newly coordinating PH_3 ligand is 2.46 Å, whereas the other Pd-P distances are 2.30 Å and 2.31 Å. The Pd-O bond of the leaving acetate ligand is 2.30 Å while the other Pd-O distance is 2.10 Å and the angle between acetate groups is 140.18°. In the weakly bound complex [**08a_INT**] after the exchange of PH_3 by AcO^-, the dissociated acetate

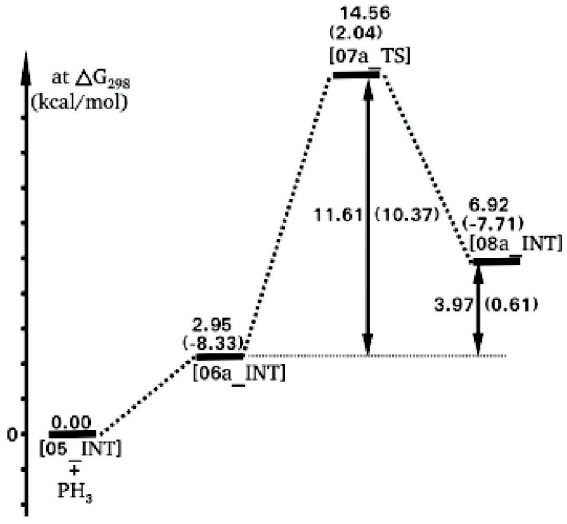

Fig. 7. Reaction profile for third addition of PH_3 ligand in the associative pathway. Relative free energies are given for each states in the reaction. The numbers in parentheses are relative total energies. Energies are in kcal mol^{-1}.

is away from the Pd(II) center (Pd-O distance is 2.98 Å) which is longer than coordinated/intermediate distances (2.2/2.4 Å).

The ligand exchange process, going from [**06a_INT**] to [**08a_INT**], is exothermic ($\Delta_r E$ = –7.71 kcal mol^{-1}; $\Delta_r E^{DMF}$ = –9.49 kcal mol^{-1}), but endergonic ($\Delta_r G$ = 6.92 kcal mol^{-1}; $\Delta_r G^{DMF}$ = 5.14 kcal mol^{-1}) considering the free reactants, [**05_INT**] and PH_3. The geometries of the intermediates, [**06a_INT**], [**07a_TS**], and [**08a_INT**], in this step and their relevant parameters are shown in Fig. 8.

The [**08a_INT**] can be dissociated into either cationic complex and anionic ligands or anionic complex and cationic ligands. The formation of two ionic species from a neutral species usually shows high endothermicity due to the artifacts in treating the ionic species computationally in gas phase. The continuum solvation models usually bring this down to some extent. The products of this step in the first case (eq. (3)) is $[Pd(PH_3)_3(OAc)]^+$ (**[09a_INT]$^+$**) and acetate anion. This step is highly endergonic. The free energies of reaction for these steps are 152.38 kcal mol^{-1} in gas phase and 40.72 kcal mol^{-1} in DMF (COSMO).

$$[\mathbf{08a\_INT}] \rightarrow [Pd(OAc)(PH_3)_2]^+ + AcO^- \quad (3)$$

The second possible dissociation of [**05_INT**] is an intramolecular reduction to form $[PPh_3\text{-}Pd\text{-}OAc]^-$ ([**06d_INT**]$^-$) and $[PH_3\text{-}OAc]^+$ shown in eq. (4). This is slightly more endergonic, 158.78 kcal mol^{-1} compared to eq. (3). Here also, solvation bring down the free energy change to 46.33 kcal mol^{-1}. The [**06d_INT**]$^-$ is linear Pd(0) complex coordinates with acetate and phosphine ligands. The bond distances of Pd-O and Pd-P are 2.09 Å and 2.12 Å respectively. The angle is 176.0°, and the acetate coordination is η^1 instead of η^2.

$$[\mathbf{08a\_INT}] \rightarrow [AcO\text{-}PH_3]^+ + [Pd(OAc)(PH_3)]^- \quad (4)$$

The subsequent addition of phosphine (PH_3) to [**06d_INT**]$^-$ yields the tri-coordinated anionic complex [**07d_INT**]$^-$, a trigonal planar structure (eq. (5)). Both are active catalysts in catalytic reactions. In [**07d_INT**]$^-$, Pd-P bonds distance are different 2.19 Å and 2.30 Å. The reaction energy of third phosphine addition to the [**06d_INT**]$^-$ is –14.33 kcal mol^{-1} (–8.73 in DMF solvent) and free energy is –3.36 kcal mol^{-1} (2.25 in DMF solvent). The structural parameters and energy values along with optimized geometries are shown in Fig. 9.

$$[Pd(OAc)(PH_3)]^- + PH_3 \rightarrow [Pd(OAc)(PH_3)_2]^- \quad (5)$$

The addition of another PH_3 to the [**07d_INT**]$^-$ (eq. (6)) is also favorable and the reaction energy is –6.04 kcal mol^{-1}

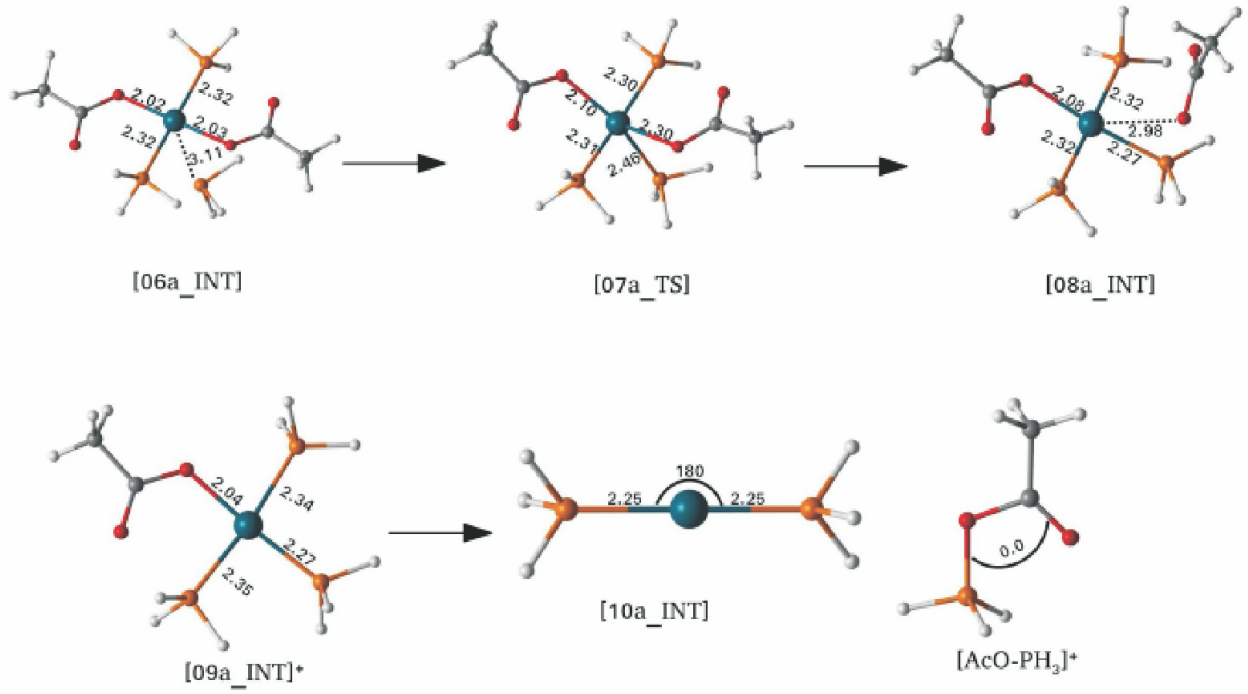

Fig. 8. Intermediates in the associative mechanism for the ligand exchange in [**05_INT**], in which the acetate ligand is replaced by a PH_3 ligand.

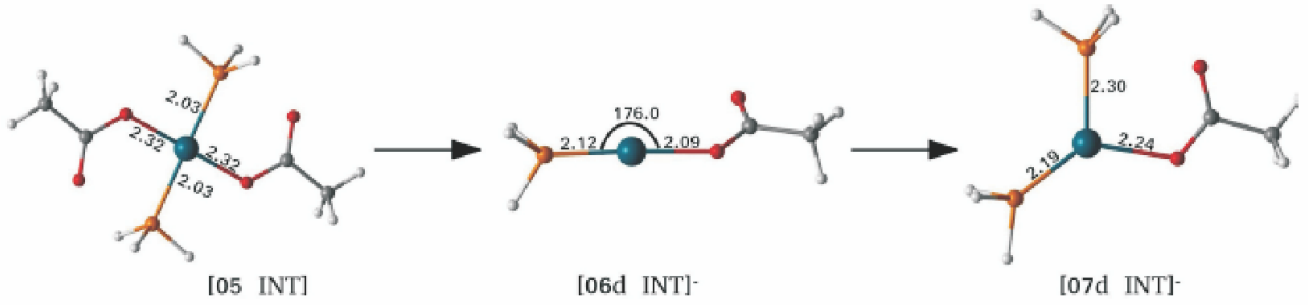

Fig. 9. Dissociated mechanism in third addition of PH_3 ligand.

(–2.79 in DMF). The resultant complex ([**08d_INT**]$^-$) is a tetraco-ordinated anionic complex shown in Fig. 10. The complex has a tetrahedral geometry at Pd(0) center and is an 18 electron system.

$$[Pd(OAc)(PH_3)_2]^- + PH_3 \rightarrow [Pd(OAc)(PH_3)_3]^- \quad (6)$$

Further addition of PH_3 to [**08d_INT**]$^-$ requires the removal of the last acetate ion. The exchange of acetate by phosphine (eq. (7)), resulting in [**12_INT**], is endergonic in gas phase and in DMF. The overall ligand exchange involves two intermediate weakly bound complexes, [**09d_INT**]$^-$ in which the incoming PH_3 is bound to [**08d_INT**]$^-$ and [**10d_INT**]$^-$ in which the leaving acetate ion is bound to [**12 INT**].

$$[Pd(OAc)(PH_3)_3]^- + PH_3 \rightarrow [Pd(PH_3)_4] + OAc^- \quad (7)$$

The first bound complex [**09d_INT**]$^-$ has a distorted trigonal bi-pyramidal geometry. One of the phosphines and the acetate ligand are in axial position, and the other three phosphine ligands are in equatorial positions. The axial acetate ligand is bonded to Pd(0) center with Pd-O distance of 2.33 Å. The Pd-P distances with equatorial phosphines are 2.35 Å, 2.27 Å, and 2.28 Å. The axial phosphine is weakly bound with a Pd-P bond distance of 3.45 Å. The stabilization attained by the binding of PH_3 in complex [**09d_INT**]$^-$ is –9.27 kcal mol^{-1} (–5.40 in DMF), but the free energy is increased by 3.75 kcal mol^{-1} (7.62 in DMF). Optimized geometries along with relevant structural parameters are shown in Fig. 10. The transition state [**10d_TS**]$^-$ for this associative ligand exchange is shown in Fig. 10. In [**10d_TS**]$^-$, the new Pd-P bond distance is 2.92 Å and simultaneously elongated Pd-O bond distance is 2.91 Å. The reaction profile for this step is shown in Fig. 10. The second bound complex [**11d_INT**]$^-$ after the

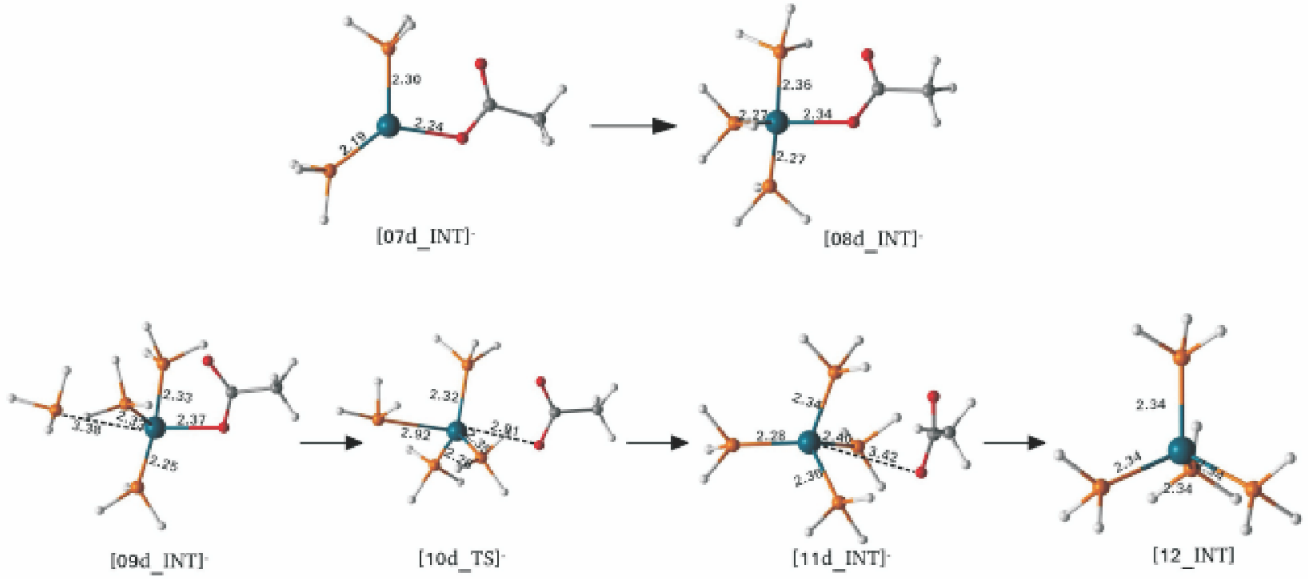

Fig. 10. Formation of tetraphosphine palladium(0) catalyst from dissociative pathway.

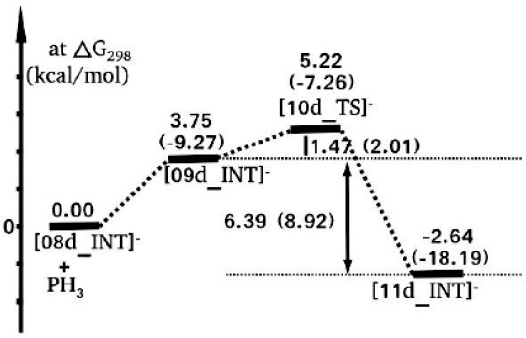

Fig. 11. Reaction profile for fifth addition of PH_3 ligand in dissociative pathway. Relative free energies are given for each states in the reaction. The numbers in parentheses are relative total energies. Energies are in kcal mol^{-1}.

transition state has the acetate weakly bound. [**11d_INT**]$^-$ is more stable than [**09d_INT**]$^-$ by 8.82 kcal mol^{-1}.

The other dissociation product of [**08d_INT**]$^+$ is [**09a_INT**]$^+$ (eq. (3)). The sp^2 oxygen of acetate ligand is oriented towards one of the PH_3 ligands in [**09a_INT**]$^+$, and this phosphine makes an angle of 94.49°, while the other PH_3 is closer to the acetate. The third PH_3 that is in *trans* position to the acetate make an angle of 175.95°. The Pd-P bond distances are higher (2.34 Å and 2.35 Å) with the *cis*-PH_3 compared with *trans*-PH_3 (2.27 Å) because of the electron withdrawing effect of the acetate in the *trans* position.

In next step, the intramolecular reduction of the intermediate complex [**09a_INT**]$^+$ into the bis-phosphine palladium(0) complex ([**10a_INT**] and the [**PH_3-OAc**]$^+$ (eq. (3)). The resultant intermediate is bis-phosphine palladium(0) neutral complex [**10a_INT**] which is one of the active pre-catalyst that initiates the catalytic cycle. The optimized geometries are shown in Fig. 8. The [**10a_INT**] has linear geometry with bond distances between Pd-P is 1.59 Å and angle is 179.9°. The [**PH_3-OAc**]$^+$ is tetrahedral at phosphorous center, the P-O bond length is 1.63 Å and P-O-C-C dihedral angle is 0°. The other conformation with the dihedral of 178.4° is –8.56 kcal mol^{-1} (–3.98 kcal mol^{-1} in DMF). The oxidation state of the palladium is +II in [**09a_INT**]$^+$ and, it is a 16 electron system. The energy and Gibbs free energy of reaction for this step are 60.87 kcal mol^{-1} (38.11 kcal mol^{-1} in DMF).

$$[Pd(OAc)(PH_3)_3]^+ \rightarrow Pd(PH_3)_2 + [AcO\text{-}PH_3]^- \quad (8)$$

Further additions of PH_3 to bis-phosphine complex, [**10a_INT**], lead to tri-coordinated complex $Pd(PH_3)_3$ ([**11a_INT**]). The [**11a_INT**] has a trigonal planar geometry and is a 16 electron system. The reaction energy of this step is –10.38 kcal mol^{-1} (–6.93 upon solvation).

$$Pd(PH_3)_2 + PH_3 \rightarrow Pd(PH_3)_3 \quad (9)$$

Finally, the formation of tetra-phosphine palladium(0) catalyst by adding one more phosphine to [**11a_INT**] is favorable as the step is barrier less and is exothermic by –5.11 kcal mol^{-1} (–3.46 in DMF). The 18 electron complex tetra-coordinated palladium catalyst has tetrahedral geometry with equal bond lengths between Pd(0) and phosphine (2.34 Å). The optimized geometries along with structural parameters are shown in Fig. 12.

The Gibbs free energy of formation of tetraphosphine Pd(0) catalyst from the [**10a_INT**] is –15.49 kcal mol^{-1} (–10.38 in DMF). As expected, energies for fourth PH_3 addition to the [**10a_INT**] and fifth PH_3 addition to [**11a_INT**] are similar with PPh_3 as a ligand reported by Kegl *et al.*[28]. From

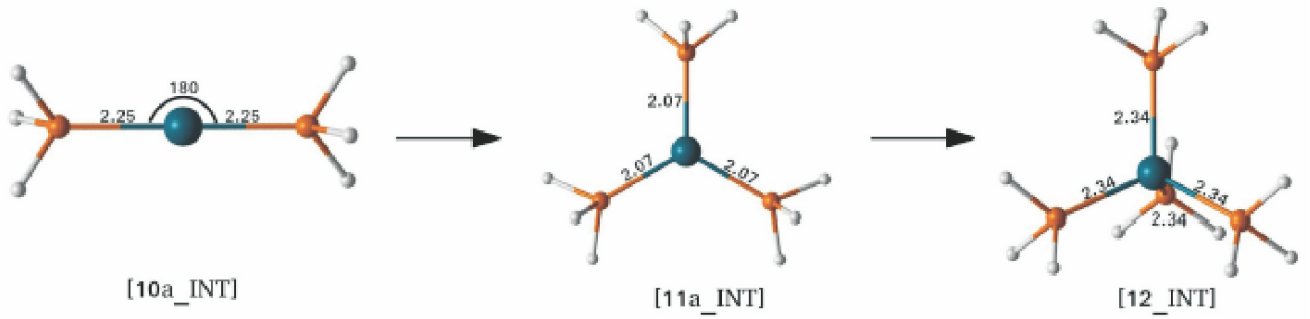

Fig. 12. Formation of tetraphosphine palladium(0) catalyst from associated mechanism pathway.

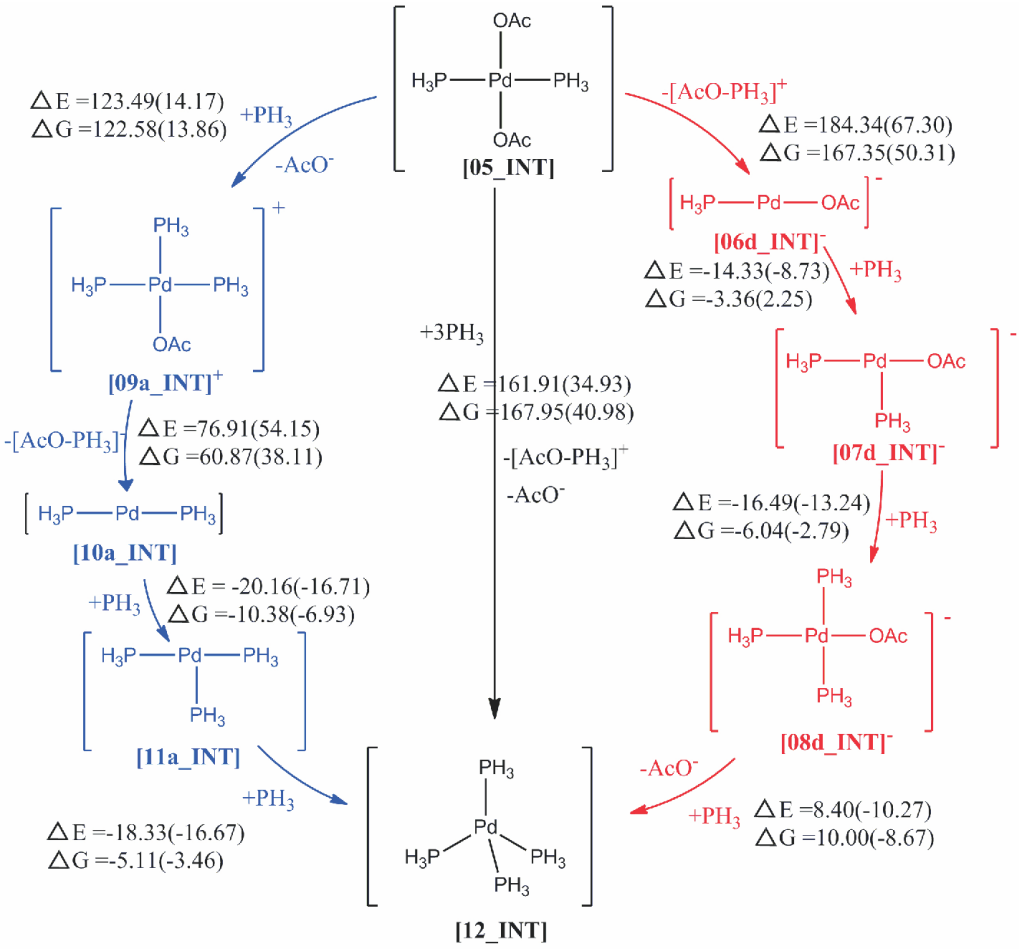

Fig. 13. The steps in the formation of active catalyst species.

these results, the DMF solvent was more effective than without solvents.

Conclusion

The formation of active catalyst species in the Pd-catalyzed reactions is studied using Density Functional Theory calculations. Palladium acetate, Pd(II)$(OAc)_2$, with phosphines used in several coupling reactions such as Heck reaction undergoes a series of steps to form reactive Pd(0) species that acts in the catalytic cycle. The steps are addition, dissociation, or ligand-exchange reactions. The ligand-exchange can occur either through associative mechanism or dissociative mechanism. We have calculated the reaction energies for all the steps, and activation barriers for associative ligand exchange steps. Two consecutive addition of two phosphines (PH_3) to $PdOAc_2$ to form $Pd(OAc)_2(PH_3)_2$ are exergonic steps. In these steps, one of the Pd-O bonds of acetate is replaced by Pd-P bond. The barriers are 8.16 kcal mol^{-1} and 5.33 kcal mol^{-1}.

There are many possibilities for next steps that lead to various active catalyst species. We have calculated the reaction energies for all these steps. The barriers for the associative exchange of acetate by PH_3 in $Pd(OAc)_2(PH_3)_2$ is 14.56 kcal mol^{-1}. Another such ligand exchange in $[Pd(OAc)(PH_3)_3]^-$ has the barrier 5.22 kcal mol^{-1}. Exchange reactions on neutral species that yields ionic species are endothermic. The inclusion of solvation effects with COSMO continuum solvation models have large effects in such reactions. The addition of phosphines are exothermic. The dissociative steps are the removal of acetate anion, AcO^-, or intramolecular dissociation of $[AcO\text{-}PH_3]^+$. This study is a

basis for future studies of the active catalyst formation of various such catalysts involving different ligands.

Acknowledgements

We acknowledge the support of the Science and Engineering Research Board, Department of Science and Technology, India through the EMR grant No. EMR/2017/003048, and DST, India for the computational facilities through the FIST grants (SR/FST/CSII-026/2013 and SR/FST/CSII-011/2005). DYR thank UGC for fellowship.

References

1. R. F. Heck, *J. Am. Chem. Soc.,* 1969, **91(24)**, 6707. https://doi.org/10.1021/ja01052a029.
2. R. F. Heck and J. P. Nolley, *J. Org. Chem.,* 1972, **37(14)**, 2320. https://doi.org/10.1021/jo00979a024.
3. E.-i. Negishi and S. Baba, *J. Chem. Soc., Chem. Commun.,* 1976, **15**, 596b. https://doi.org/10.1039/c3976000596b.
4. E. Negishi, A. O. King and N. Okukado, *J. Org. Chem.,* 1977, **42(10)**, 1821. https://doi.org/10.1021/jo00430a041.
5. N. Miyaura and A. Suzuki, *J. Chem. Soc., Chem Commun.,* 1979, **19**, 866. https://doi.org/10.1039/c39790000866.
6. N. Miyaura, K. Yamada and A. Suzuki, *Tetrahedron Lett.,* 1979, **20(36)**, 3437. https://doi.org/https://doi.org/10.1016/S0040-4039(01)95429-2.
7. N. Miyaura and A. Suzuki, *Chem. Rev.,* 1995, **95(7)**, 2457. https://doi.org/10.1021/cr00039a007.
8. J. K. Stille, *Angew. Chem. Int. Ed. Eng.,* 1986, **25(6)**, 508. https://doi.org/10.1002/anie.198605081.
9. T. Sperger, H. C. Fisher and F. Schoenebeck, *Wiley Interdisciplinary Reviews: Computational Molecular Science,* 2016, **6(3)**, 226. https://doi.org/10.1002/wcms.1244.
10. C. Amatore, A. Jutand and M. A. M'Barki, *Organometallics,* 1992, **11(9)**, 3009. https://doi.org/10.1021/om00045a012.
11. C. Amatore, E. Carre, A. Jutand and M. A. M'Barki, *Organometallics,* 1995, **14(4)**, 1818. https://doi.org/10.1021/om00004a039.
12. C. Amatore, E. Carre, A. Jutand, Mohamed Amine M'Barki and G. Meyer, *Organometallics,* 1995, **14(12)**, 5605. https://doi.org/10.1021/om00012a029.
13. C. Amatore and A. Jutand, *J. Org. Chem.,* 1999, **576(1)**, 254. https://doi.org/https://doi.org/10.1016/S0022-328X(98)01063-8.
14. C. Amatore and A. Jutand, *Acc. Chem. Res.,* 2000, **33(5)**, 314. https://doi.org/10.1021/ar980063a.
15. N. Thirupathi, D. Amoroso, A. Bell and J. D. Protasiewicz, *Organometallics* 2005, **24(17)**, 4099. https://doi.org/10.1021/om050356p.
16. N. Thirupathi, D. Amoroso, A. Bell and J. D. Protasiewicz, *Organometallics,* 2007, **26(13)**, 3157. https://doi.org/10.1021/om070069g.
17. Q. Zheng, Y. Liu, Q. Chen, M. Hu, R. Helmy, E. C. Sherer, C. J. Welch and H. Chen, *J. Am. Chem. Soc.,* 2015, **137(44)**, 14035. https://doi.org/10.1021/jacs.5b08905.
18. C. L. McMullin, J. Jover, J. N. Harvey and N. Fey, *Dalton Trans.,* 2010, **39(45)**, 10833. https://doi.org/10.1039/C0DT00778A.
19. K. Vikse, T. Naka, J. S. McIndoe, M. Besora and F. Maseras, *ChemCatChem,* 2013, **5(12)**, 3604. https://doi.org/10.1002/cctc.201300723.
20. P. Vidossich, G. Ujaque and A. Lledos, *Chem. Commun.,* 2014, **50(6)**, 661. https://doi.org/10.1039/C3CC47404F.
21. M. Kolter and K. Koszinowski, *Chemistry – A European Journal,* 2016, **22(44)**, 15744. https://doi.org/10.1002/chem.201603431.
22. B. A. Anjali and C. H. Suresh, *ACS. Omega*, 2017, **2(8)**, 4196. https://doi.org/10.1021/acsomega.7b00745.
23. Y. Liang, Y.-Y. Jiang, Y. Liu and S. Bi, *Org. Biomol. Chem.,* 2017, **15(29)**, 6147. https://doi.org/10.1039/C7OB01021D.
24. T. Sperger, C. M. Le, M. Lautens and F. Schoenebeck, *Chem. Sci.,* 2017, **8(4)**, 2914. https://doi.org/10.1039/C6SC05001H.
25. M. Ahlquist and P.-O. Norrby, *Organometallics,* 2007, **26(3)**, 550. https://doi.org/10.1021/om0604932.
26. U. Christmann and R. Vilar, *Angew. Chem. Int. Ed.,* 2005, **44(3)**, 366. https://doi.org/10.1002/anie.200461189.
27. S. Kozuch, C. Amatore, A. Jutand and S. Shaik, *Organometallics,* 2005, **24(10)**, 2319. https://doi.org/10.1021/om050160p.
28. N. Palinkas, L. Kollar and T. Kegl, *Dalton Trans.,* 2017, **46(45)**, 15789. https://doi.org/10.1039/C7DT03642F.
29. C.-H. Guo and H. Jiao, "Computational Investigations into the Heck Type Reaction Mechanisms. In: Applied homogeneous catalysis with organometallic compounds", Wiley-Blackwell, 2017, pp. 951-982. https://doi.org/10.1002/9783527651733.ch12.
30. M. Besora, C. Gourlaouen, B. Yates and F. Maseras, *Dalton Trans.,* 2011, **40(42)**, 11089. https://doi.org/10.1039/C1DT10983A.
31. P. Veerakumar, P. Thanasekaran, K.-L. Lu, K.-C. Lin and S. Rajagopal, *ACS Sustainable Chemistry & Engineering,* 2017, **5(10)**, 8475. https://doi.org/10.1021/acssuschemeng.7b00922.
32. Z. Li, Y. Fu, Q.-X. Guo and L. Liu, *Organometallics,* 2008, **27(16)**, 4043. https://doi.org/10.1021/om701065f.
33. K. C. Lam, T. B. Marder and Z. Lin, *Organometallics,* 2007, **26(3)**, 758. https://doi.org/10.1021/om060784a.
34. C. Acktorp and P.-O. Norrby, *Dalton Trans.,* 2011, **4(42)**, 11308. https://doi.org/10.1039/C1DT10558B.
35. A. Bottoni, M. A. Carvajal, G. P. Miscione and J. J. Novoa, *Molecular Physics,* 2010, **108(12)**, 1619. https://doi.org/10.1080/00268976.2010.486139.

36. G. Henkelman, P. Uberuaga and Jonsson Blas, *J. Chem. Phys.,* 2000, **113(22)**, 9901. https://doi.org/10.1063/1.1329672.
37. A. Heyden, T. Bell, Keil Alexis and J. Frerich. *J. Chem. Phys.,* 2005, **123(22)**, 224101. https://doi.org/10.1063/1.2104507.
38. J. Kästner, J. M. Carr, T. W. Keal, W. Thiel, A. Wander and P. Sherwood, *J. Phys. Chem. A,* 2009, **113(43)**, 11856. https://doi.org/10.1021/jp9028968.
39. ChemShell, a Computational Chemistry Shell.
40. F. Furche, R. Ahlrichs, C. Hättig, W. Klopper, M. Sierka and F. Turbomole Weigend, *Wiley Interdisciplinary Reviews: Computational Molecular Science,* 2014, **4(2)**, 91. https://doi.org/10.1002/wcms.1162.
41. P. Deglmann, F. Furche and R. Ahlrichs, *Chem. Phys. Lett.,* 2002, ***362(5)***, 511. https://doi.org/https://doi.org/10.1016/S0009-2614(02)01084-9.
42. P. Deglmann and F. Furche, *J. Chem. Phys.,* 2002, **117(21)**, 9535. https://doi.org/10.1063/1.1523393.
43. D. M. Kenneth and P. J. James, *J. Mol. Struct. THEOCHEM,* 1988, **163**, 143. https://doi.org/https://doi.org/10.1016/0166-1280(88)80386-5.
44. J. P. Perdew, *Phys. Rev. B,* 1986, **33(12)**, 8822. https://doi.org/10.1103/PhysRevB.33.8822.
45. A. D. Becke, *Phys. Rev. A,* 1988, **38(6)**, 3098. https://doi.org/10.1103/PhysRevA.38.3098.
46. A. Schäfer, H. Horn and R. Ahlrichs, *J. Chem. Phys.,* 1992, **97(4)**, 2571. https://doi.org/10.1063/1.463096.
47. K. Eichkorn, F. Weigend, O. Treutler and R. Ahlrichs, *Theoretical Chemistry Accounts,* 1997, **97(1)**, 119. https://doi.org/10.1007/s002140050244.
48. P. J. Hay and W. R. Wadt, *J. Chem. Phys.,* 1985, **82(1)**, 299. https://doi.org/10.1063/1.448975.
49. P. J. Hay and W. R. Wadt, *J. Chem. Phys.,* 1985, **82(1)**, 270. https://doi.org/10.1063/1.448799.
50. C. Lee, W. Yang, G. Parr and Robert, *Phys. Rev. B,* 1988, **37(2)**, 785. https://doi.org/10.1103/PhysRevB.37.785.
51. Y. Zhao and D. G. Truhlar, *Theoretical Chemistry Accounts,* 2008, **120(1)**, 215. https://doi.org/10.1007/s00214-007-0310-x.